MNRAS **000**, 000–000 (0000) Preprint 16 January 2019 Compiled using MNRAS LATEX style file v3.0

The strong lens line-of-sight structure and substructure challenge: challenge design

The Challenge Team

16 January 2019

ABSTRACT

We describe the setup of a multi-tiered challenge to accurately infer the line-of-sight structure and substructure content in strong galaxy-galaxy lens systems from simulated optical or radio telescope data.

1 OVERVIEW OF THE CHALLENGE SETUP

The challenge is divided into four levels of increasing difficulty, complexity, and/or realism from level 0 (simple source, simple main lens mass, single substructure, simple instrument without noise, all parameters known) to level 3 (complex source, complex main lens, multiple l.o.s. structures and substructures, realistic instruments).

1.1 All levels

The models and parameters common to several/all challenge levels are:

- The **cosmology** for distance calculations is a flat ΛCDM model with parameters $\Omega_\Lambda = 0.7$, $\Omega_\mathrm{m} = 1 - \Omega_\Lambda = 0.3$, $H_0 = 70\,\mathrm{km\,s^{-1}\,Mpc^{-1}}$.
- The **main lens redshift** $z_\mathrm{d} = 0.6$.
- The **source redshift** $z_\mathrm{s} = 2.5$.
- The **mass of the main lens** for all systems is chosen such that the Einstein radius is between 0.7 and 2 arcsec.
- The **optical images** have an area of $10 \times 10\,\mathrm{arcsec}^2$ and pixels of approx. $0.01 \times 0.01\,\mathrm{arcsec}^2$.
- The **simple noise in optical images** at the lower levels is modelled as uncorrelated normally distributed pixel noise.
- The **simple point spread function** (psf) for the optical data at the lower levels is modelled as a two-dimensional normal distribution with FWHM of approx. 0.06 arcsec.
- The **simple source** light distributions at the lower levels are modelled as a elliptical Sersic profiles with parameters drawn from simple distributions compatible with data from Oldham et al. (2017).
- The **simple main lenses** at the lower levels are modelled as a singular power-law ellipsoid (SPLE, Barkana 1998; Koopmans et al. 2003) plus a spatially constant external shear with parameters drawn from distributions compatible with Oldham et al. (2017).
- **Line-of-sight (l.o.s.) structures** are modelled as spherical NFW halos (Navarro et al. 1996, 1997).
- **Substructures** are modelled as smoothly truncated spherical NFW halos (Baltz et al. 2009) with truncation radii larger than their virial radii.
- The **substructure masses** M_200c for single-substructure systems are drawn from distributions uniform in $\log_{10}(M_\mathrm{200c}/\mathrm{M}_\odot)$ in the range $[5.5, 7]$ for low-S/N systems, $[7, 8.5]$ for medium-S/N systems, and $[8.5, 10]$ for high-S/N systems.
- The **l.o.s. mass function** (from which l.o.s. halo masses are drawn at higher challenge levels) is modelled as Sheth & Tormen (1999) mass function modified by a factor $F \in [5, 20]$.
- The **substructure mass function** (from which substructure masses are drawn at higher challenge levels) is modelled as a power law $n(>M) \propto M^{-1.93}$ with an amplitude according to (Sawala et al. 2017; Despali et al. 2018) modified by an amplitude factor $F \in [5, 20]$.
- The **l.o.s. mass-concentration relation** and **substructure mass-concentration relation** (from which l.o.s. and substructure concentrations are drawn) are modelled as a log-normal distribution in concentration for fixed mass (Neto et al. 2007; Hellwing et al. 2016).

1.2 Challenge level 0

This level is provided as a check of the basic functionality of the interface to the simulated data and lens modelling software.

- **number** of lens systems: 1 system with large Einstein radius (i.e. between 1 and 2 arcsec) and 1 system with small (below 1 arcsec) Einstein radius (all model types known, all parameters known)
- **source**: Sersic elliptical
- **main lens mass**: SPLE + external shear
- **main lens light**: none (orientation of main lens mass provided explicitly)
- **substructure**: 1 significant (i.e. high signal-to-noise ratio) smoothly truncated spherical NFW
- **line-of-sight structure**: none
- **optical data**: real space image with simple PSF and without and with simple pixel noise + noise statistics
- **radio data**: list of amplitudes at certain harmonic space vectors without and with simple noise + noise statistics
- **goal**: confirmation that provided 'true' parameters of main lens, substructure, and source are recovered
- **timeline**: mock data provided to modellers by Jan 2019

1.3 Challenge level 1

This level is the first one where unknown parameters need to be inferred.

- **number** of lens systems: 6 large + 6 small (all model types known, all parameter priors known, parameter values unknown)
- **source**: Sersic elliptical
- **main lens mass**: SPLE + external shear
- **main lens light**: none, but prior on ellipticity and orientation of main lens mass provided as would be inferred from a light ellipticity
- **substructure**: 1 smoothly truncated spherical NFW per system, 4 systems with high-S/N substructure, 4 mid-S/N, 4 low-S/N
- **line-of-sight structure**: none
- **optical data**: real space image with simple PSF and with simple pixel noise + noise statistics
- **radio data**: list of amplitudes at certain harmonic space vectors with simple noise + noise statistics
- **goal**: parameters of main lens, substructure, and source
- **timeline**: mock data provided to modellers by Jan 2019, parameter unblinding 2019 March 31, modellers frequently interact in between

1.4 Challenge level 2

This level is the first one with realistic sources and a population of substructures and l.o.s. structures.

- **number** of lens systems: 10 blind (all model types known, all parameter priors known, parameter values unknown) + 10 non-blind (all model types known, all parameters known, source provided)
- **optical source**: realistic (hi-res. low-z galaxy image modified to mock high-z galaxy, provided by M. Auger)
- **radio source**: realistic (real source or set of blobs provided by D. Marrone and/or J. McKean)
- **main lens mass**: SPLE + external shear
- **main lens light**: none, but prior on ellipticity and orientation of main lens mass provided as would be inferred from a light ellipticity
- **substructure**: population of smoothly truncated spherical NFWs with masses sampled from substructure mass function with unknown amplitude modification factor F and concentrations sampled from substructure mass-concentration relation
- **line-of-sight structure**: population of spherical NFWs with masses sampled from l.o.s. mass function with unknown amplitude modification factor F and concentrations sampled from l.o.s. mass-concentration relation
- **optical data**: real space image with simple PSF and with simple pixel noise + noise statistics
- **radio data**: list of amplitudes at certain harmonic space vectors with simple noise + noise statistics
- **goal**: parameters of main lens, source, mass function amplitude F, and parameters of any individually detected l.o.s. and substructure
- **timeline**: mock data provided to modellers by (estimated) 2019 March 31, modellers frequently interact in between

1.5 Challenge level 3

This level features realistic sources, lenses (from a simulation), a population of substructures and l.o.s. structures, and realistic instruments.

- **number** of lens systems: 10 blind (all model types known, all parameter priors known, parameter values unknown) + 10 non-blind (all model types known, all parameters known, source provided)
- **optical source**: realistic (hi-resolution low-z galaxy image modified to mock high-z galaxy)
- **radio source**: realistic
- **main lens mass**: filtered and rescaled mass distribution of galaxy from CLUELENS simulation
- **main lens light**: filtered and rescaled light distribution of galaxy from CLUELENS simulation
- **substructure**: smoothly truncated spherical NFWs with positions, masses, and concentrations (giving same $v_{\rm max}$ and $r_{\rm max}$) from CLUELENS simulation with masses modified by appropriate function of amplitude factor F such that the substructure mass function is scaled by F
- **line-of-sight structure**: population of spherical NFWs with masses sampled from l.o.s. mass function with unknown amplitude modification factor F and concentrations sampled from l.o.s. mass-concentration relation
- **optical data**: real space image with state-of-the-art realistic PSF and noise
- **radio data**: amplitudes at set of harmonic wave vectors with state-of-the-art U-V-coverage pattern and realistic noise
- **goal**: parameters of main lens, source, mass function amplitude F, and parameters of any individually detected l.o.s. and substructure
- **timeline**: mock data provided to modellers by 2019 fall

2 DETAILED DESCRIPTION

Here, we describe in more detail the models, their parameters, and the prior distributions of the model parameters for the sources and lenses in the challenge. We also give a more detailed description of the resolution and noise properties of the simulated observations.

2.1 Cosmology

We assume flat ΛCDM model with cold dark matter and a cosmological constant as background csomology. The energy density for the cosmological constant in units of the critical density $\Omega_\Lambda = 0.7$, the cosmic mean matter density parameter $\Omega_{\rm m} = 1 - \Omega_\Lambda = 0.3$, and the Hubble constant $H_0 = 70\,{\rm km\,s^{-1}\,Mpc^{-1}}$.

For simplicity, we assume a flat sky. Unless stated otherwise, positions on the sky are specified employing a right-handed Cartesian coordinate system with the origin at the center of the main lens.

2.2 The simple source

The source is assumed to have a fixed known redshift $z_{\rm s} = 2.5$. At the lower levels of the challenge, the source light

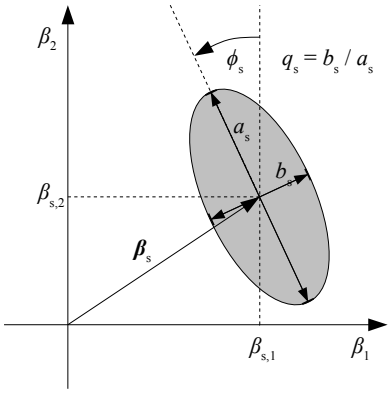

Figure 1. Schematic view of the coordinate system and parameters used to describe an elliptical source: a right-handed Cartesian coordinate system with coordinates β_1 and β_2, and an elliptical source with center at $\boldsymbol{\beta}_\mathrm{s} = (\boldsymbol{\beta}_{\mathrm{s},1}, \boldsymbol{\beta}_{\mathrm{s},2})^\mathrm{T}$, major axis a_s, minor axis b_s, axis ratio $q_\mathrm{s} = b_\mathrm{s}/a_\mathrm{s}$, and position angle ϕ_s (here $\phi_\mathrm{s} > 0$).

distribution $I_\mathrm{s}(\boldsymbol{\beta})$ as function of source angle $\boldsymbol{\beta}$ is modelled as an elliptical Sersic profile:

$$I_\mathrm{s}(\boldsymbol{\beta}; I_{\mathrm{s},0}, \boldsymbol{\beta}_\mathrm{s}, \beta_{\mathrm{s,eff}}, n_\mathrm{s}, q_\mathrm{s}, \phi_\mathrm{s}) = I_\mathrm{s}^{(0)} \times \exp\left(-k_\mathrm{s}(n_\mathrm{s})\left\{\left[\frac{r_\mathrm{eq}(\boldsymbol{\beta}-\boldsymbol{\beta}_\mathrm{s}, q_\mathrm{s}, \phi_\mathrm{s})}{\beta_{\mathrm{s,eff}}}\right]^{1/n_\mathrm{s}} - 1\right\}\right). \quad (1)$$

Here, $I_{\mathrm{s},0}$ denotes a global source brightness amplitude, $\boldsymbol{\beta}_\mathrm{s}$ denotes the position of the source center, $\beta_{\mathrm{s,eff}}$ denotes the half-light radius of the source, and n_s the Sersic index of the source. The equivalent radius

$$r_\mathrm{eq}(\boldsymbol{\beta}, q_\mathrm{s}, \phi_\mathrm{s}) = \sqrt{\boldsymbol{\beta}^\mathrm{T}\mathsf{R}(\phi_\mathrm{s})\mathsf{Q}(q_\mathrm{s})\mathsf{R}(-\phi_\mathrm{s})\boldsymbol{\beta}}. \quad (2)$$

The rotation matrix

$$\mathsf{R}(\phi_\mathrm{s}) = \begin{pmatrix} \cos(\phi_\mathrm{s}) & -\sin(\phi_\mathrm{s}) \\ \sin(\phi_\mathrm{s}) & \cos(\phi_\mathrm{s}) \end{pmatrix}, \quad (3)$$

i.e. $\mathsf{R}(-\phi_\mathrm{s})\boldsymbol{\beta}$ rotates $\boldsymbol{\beta}$ clockwise by the source position angle ϕ_s, which we define as the counter-clockwise angle between the positive β_2-direction and the sources major axis. The diagonal matrix $\mathsf{Q}(q_\mathrm{s}) = \mathsf{diag}(q_\mathrm{s}^{-1}, q_\mathrm{s})$ with source axis minor-to-major-axis ratio q_s.

The function $k_\mathrm{s}(n_\mathrm{s})$ ensures that half the total light of the source is contained inside the isophote defined by $r_\mathrm{eq}(\boldsymbol{\beta} - \boldsymbol{\beta}_\mathrm{s}, q_\mathrm{s}, \phi_\mathrm{s}) = \beta_{\mathrm{s,eff}}$. It is thus given by the solution to the equation $\Gamma(2n_\mathrm{s}, 0) = 2\Gamma[2n_\mathrm{s}, k_\mathrm{s}(n_\mathrm{s})]$, where Γ denotes the upper incomplete gamma function.

The source brightness amplitude $I_{\mathrm{s},0}$ is drawn from a uniform distribution in the interval $[2.5, 3]$ in units of the optical image pixel noise level $\sigma_{\mathrm{n,pix}}$. (tests show that this yields signal-to-noise ratios ~ 10 in the noisy optical images for the current setup). The source center $\boldsymbol{\beta}_\mathrm{s}$ is drawn from a uniform distribution within circular region the source plane such that $|\boldsymbol{\beta}_\mathrm{s}| \leqslant 0.5\,\mathrm{arcsec}$. The half-light radius $\beta_{\mathrm{s,eff}}$ is drawn from a uniform distribution in the interval $[0.1, 0.5]$ arcsec (roughly consistent with Newton et al. 2011). The Sersic index n_s is drawn from a uniform distribution in the interval $[0.8, 2.2]$. The source axis ratio q_s is drawn from a normal distribution with mean 0.6 and standard deviation 0.15, truncated to the interval $[0.2, 1]$. The position angle is ϕ_s drawn from a uniform distribution in the interval $[-\pi/2, \pi/2)$.

2.3 The simple main lens

The main lens is assumed to have a fixed known redshift $z_\mathrm{d} = 0.6$. Its center defines the origin of the lens plane (and its image position defines the origin of the image plane). The projected mass distribution of the main lens at the lower levels is assumed to follow a singular power-law ellipsoidal profile (SPLE, Barkana 1998; Koopmans et al. 2003):

$$\Sigma_\mathrm{d}(\boldsymbol{\theta}; \theta_\mathrm{E}, \gamma'_\mathrm{d}, q_\mathrm{d}, \phi_\mathrm{d}) = \Sigma_\mathrm{cr}(z_\mathrm{d}, z_\mathrm{s})\frac{3-\gamma'_\mathrm{d}}{2}\left[\frac{r_\mathrm{eq}(\boldsymbol{\theta}, q_\mathrm{d}, \phi_\mathrm{d})}{\theta_\mathrm{E}}\right]^{1-\gamma'_\mathrm{d}}. \quad (4)$$

Here, θ_E denotes the main lens Einstein radius, γ'_d denotes the power law slope parameter of the profile, q_d denotes the main lens surface density's axis ratio, and ϕ_d denotes the main lens position angle. The mean surface mass density inside the ellipse $r_\mathrm{eq}(\boldsymbol{\theta}; q_\mathrm{d}, \phi_\mathrm{d}) = \theta_\mathrm{E}$ equals the critical surface mass density

$$\Sigma_\mathrm{cr}(z_\mathrm{d}, z_\mathrm{s}) = \left[\frac{4\pi\mathrm{G}}{\mathrm{c}^2}\frac{D(z_\mathrm{d})D(z_\mathrm{d}, z_\mathrm{s})}{D(z_\mathrm{s})}\right]^{-1}, \quad (5)$$

where G denotes Newton's gravitational constant, c denotes the speed of light, and D denotes the angular diameter distance.

The Einstein radius θ_E is drawn from a uniform distribution in the interval $[0.7, 1]$ arcsec for small systems and in the interval $[1, 2]$ arcsec for large systems. The power law slope parameter γ'_d is drawn from a normal distribution with mean 2.1 and standard deviation 0.1, truncated to the interval $[1.5, 2.8]$.

The light distribution of the main lens is not directly included in the simulated images. Instead, its axis ratio q_l and position angle ϕ_l are provided as auxiliary information to infer the main lens mass density. The main lens light axis ratio q_l is drawn from a uniform distribution in the interval $[0.6, 0.95]$. The main lens light position angle ϕ_l is drawn from a uniform distribution in the interval $[-\pi/2, \pi/2)$.

The main lens surface mass density axis ratio q_d is drawn from a normal distribution with mean equal to the light axis ratio q_l and standard deviation 0.05, truncated to the interval $[0.5, 1]$. The surface mass position angle ϕ_d is drawn from a normal distribution with mean equal to the light position angle ϕ_l and standard deviation 10 deg, wrapped to the interval $[-\pi/2, \pi/2)$.

In addition to the light deflection induced by the matter distribution (4), the main lens model also includes an external shear $\gamma_\mathrm{ext} = \gamma_{\mathrm{ext},1} + \mathrm{i}\gamma_{\mathrm{ext},2}$. The external shear is drawn from a circularly symmetric bivariate normal distribution with standard deviations $\sigma_{\gamma_{\mathrm{ext},1}} = \sigma_{\gamma_{\mathrm{ext},2}} = 0.06$ restricted to $|\gamma_\mathrm{ext}| < 0.5$ (Bolton et al. 2008). We do not include an external convergence κ_ext in the main lens model.

2.4 Line-of-sight structures

Line-of-sight structures are modelled as spherically symmetric Navarro-Frenk-and-White halos (NFW, Navarro et al. 1996, 1997). Their three-dimensional matter density profile $\rho(r)$ as function of radius r reads:

$$\rho(r; z, M_{200\mathrm{c}}, c_{200\mathrm{c}}) = \frac{\rho_\mathrm{cr}(z)\delta_{200}(c_{200\mathrm{c}})r_\mathrm{s}(z, M_{200\mathrm{c}}, c_{200\mathrm{c}})^3}{r\left[r + r_\mathrm{s}(z, M_{200\mathrm{c}}, c_{200\mathrm{c}})\right]^2}, \quad (6)$$

where z denotes the halo redshift, M_{200c} denotes the halo mass, and c_{200c} the halo concentration parameter. The critical density for a flat ΛCDM universe

$$\rho_{cr}(z) = \frac{3H_0^2}{8\pi G}\left[(1+z)^3\Omega_m + \Omega_\Lambda\right] \tag{7}$$

The characteristic overdensity

$$\delta_{200}(c_{200c}) = \frac{200}{3}\frac{c_{200c}^3}{\ln(1+c_{200c}) - c_{200c}/(1+c_{200c})}. \tag{8}$$

The scale radius

$$r_s(z, M_{200c}, c_{200c}) = r_{200c}(z, M_{200c})/c_{200c} \tag{9}$$

with the halo radius defined as the radius whithin which the mean density is 200 times the critical density. Thus

$$r_{200c}(z, M_{200c}) = \left[\frac{3}{4\pi}\frac{M_{200c}}{200\,\rho_{cr}(z)}\right]^{1/3}. \tag{10}$$

For the discussion of the lensing properties of NFW-like profiles, we define the following functions:

$$f(x) = \begin{cases} \dfrac{1}{\sqrt{1-x^2}}\operatorname{arcosh}\left(\dfrac{1}{x}\right), & x < 1, \\ 1, & x = 1, \\ \dfrac{1}{\sqrt{x^2-1}}\arccos\left(\dfrac{1}{x}\right), & x > 1, \end{cases} \tag{11}$$

$$g(x) = \begin{cases} \dfrac{f(x)-1}{1-x^2}, & x < 1, \\ 1/3, & x = 1, \\ \dfrac{1-f(x)}{x^2-1}, & x > 1, \text{ and} \end{cases} \tag{12}$$

$$h(x) = \ln\left(\frac{x}{2}\right) + f(x). \tag{13}$$

For the spherical NFW profile (6), the surface mass density $\Sigma(R)$ as a function of physical projected radius R can then be written as (e.g. Bartelmann 1996; Wright & Brainerd 2000; Golse & Kneib 2002):

$$\Sigma(R; z, M_{200c}, c_{200c}) = 2\rho_{cr}\delta_{200}r_s g(R/r_s). \tag{14}$$

The physical deflection angle $\hat{\alpha}(R)$ at physical transverse separation R between halo center and light can be written as:

$$\hat{\alpha}(R) = \frac{4G}{c^2}4\pi\,\rho_{cr}\delta_{200}r_s^2\frac{h(R/r_s)}{R/r_s}. \tag{15}$$

The convergence for sources at redshift z_s and image position $\boldsymbol{\theta}$ relative to the halo center can be written as:

$$\kappa(\boldsymbol{\theta}, z_s) = \frac{2\rho_{cr}\delta_{200}r_s}{\Sigma_{cr}(z, z_s)}\,g\big(|\boldsymbol{\theta}|/\theta_s\big), \tag{16}$$

where $\theta_s = r_s/D(z)$. The scaled deflection angle then reads:

$$\boldsymbol{\alpha}(\boldsymbol{\theta}, z_s) = \frac{4\rho_{cr}\delta_{200}r_s}{\Sigma_{cr}(z, z_s)}\frac{h\big(|\boldsymbol{\theta}|/\theta_s\big)}{\big(|\boldsymbol{\theta}|/\theta_s\big)^2}\boldsymbol{\theta}. \tag{17}$$

For given halo mass M_{200c}, the concentration c_{200c} is drawn from a log-normal distribution with logarithmic mean $\langle\log_{10}(c_{200c})\rangle = \log_{10} c_{med}(M_{200c})$, where

$$c_{med}(M_{200c}) = 11.5\left[\frac{M_{200c}}{10^{10}M_\odot} + \left(\frac{M_{200c}}{10^{10}M_\odot}\right)^2\right]^{-0.05} \tag{18}$$

consistent with Hellwing et al. (2016), and standard deviation $\sigma_{\log_{10}(c_{200c})} = 0.13$ broadly consistent with Neto et al. (2007).

The simulations of the lower challenge levels do not contain l.o.s. halos. For the higher challenge levels, we assume that the halo abundance follows a Sheth & Tormen (1999) mass function with parameters compatible with Sawala et al. (2017) and Despali et al. (2018), except its amplitude is modified by a factor F drawn from a uniform distribution in the interval $[5, 20]$. Furthermore, we assume that the spatial positions of the line-of-sight halo centers are uncorrelated.

2.5 Substructure

Substructures of the main lens galaxy at redshift z_d are modelled as smoothly truncated spherical NFW halos (Baltz et al. 2009). Their three-dimensional matter density profile reads:

$$\rho(r; M_{200c}, c_{200c}, r_t) = \frac{\rho_{cr}(z)\delta_{200}(c_{200c})r_s(z, M_{200c}, c_{200c})^3}{r\big[r + r_s(z, M_{200c}, c_{200c})\big]^2}\frac{r_t^2}{r^2 + r_t^2}, \tag{19}$$

where M_{200c} denotes the subhalo mass and c_{200c} denotes the subhalo concentration parameter of the corresponding untruncated NFW profile, and r_t denotes the truncation radius.

Besides the functions f and g defined in Section 2.4, we require:

$$k(x, t) = \ln\left(\frac{x}{\sqrt{x^2 + t^2} + t}\right), \tag{20}$$

$$l(x, t) = \frac{t^2}{(t^2+1)^2}\left[(t^2+1)g(x) + 2f(x) - \frac{\pi}{\sqrt{t^2+x^2}} + \frac{t^2-1}{t\sqrt{t^2+x^2}}k(x, t)\right], \tag{21}$$

$$m(x, t) = \frac{t^2}{(t^2+1)^2}\left[\left(t^2 + 2x^2 - 1\right)f(x) + \pi t + \left(t^2-1\right)\ln(t) + \sqrt{x^2+t^2}\left(\frac{t^2-1}{t}k(x, t) - \pi\right)\right]. \tag{22}$$

The surface mass density $\Sigma(R)$ reads then:

$$\Sigma(R; z_d, M_{200c}, c_{200c}) = 2\rho_{cr}\delta_{200}r_s l(R/r_s). \tag{23}$$

The physical deflection angle $\hat{\alpha}(R)$ at physical transverse separation R between subhalo center and light can be written as:

$$\hat{\alpha}(R) = \frac{4G}{c^2}4\pi\,\rho_{cr}\delta_{200}r_s^2\frac{m(R/r_s)}{R/r_s}. \tag{24}$$

For simplicity, we fix the truncation radius to twice the subhalo radius, i.e. $r_t = 2r_{200c}$. As for the line-of-sight halos, the concentration c_{200c} for subhalos with mass M_{200c} is drawn from a log-normal distribution with logarithmic mean given by Eq. (18) and standard deviation $\sigma_{\log_{10}(c_{200c})} = 0.13$ (Neto et al. 2007; Hellwing et al. 2016).

The simulations of the lower challenge levels contain only a single subhalo. The subhalo position is drawn from a uniform distribution within the region where $0.7\,\text{arcsec} \leqslant \boldsymbol{\theta} \leqslant 1\,\text{arcsec}$ for small systems and $1\,\text{arcsec} \leqslant \boldsymbol{\theta} \leqslant$

2 arcsec for large systems. In addition, we enforce that image signal-to-noise ratio near the subhalo position is at least 3 by discarding any systems not satisfying this criterion. The subhalo mass is drawn from distributions uniform in $\log_{10}(M_{200c}/M_\odot)$ in the range $[5.5, 7]$ for low-S/N systems, $[7, 8.5]$ for medium-S/N systems, and $[8.5, 10]$ for high-S/N systems.

For systems at challenge level 2, we assume a spatially uniform distribution of subhalos in projection across the whole field of view with a surface number density $n(> M_{200c})$ of subhalos above a given mass M_{200c} following a power law:

$$n(> M_{200c}) = F\, n_0 \left(\frac{M_{200c}}{10^{10}\,M_\odot} \right)^{-1.93} . \quad (25)$$

The amplitude n_0 is chosen in accordance with Sawala et al. (2017); Despali et al. (2018). The amplitude modification factor F is the same as for the line-of-sight halo abundance, which is drawn from a uniform distribution in the interval $[5, 20]$.

2.6 Optical images

The optical images are quadratic with a side length of 10 arcsec covered by 1024 pixels per dimension. The images are centred on the main lens. For the lower challenge levels, the effects of the point-spread function are modelled as a convolution with a circularly symmetric bivariate normal distribution with standard deviation per dimension $\sigma_{psf,1} = \sigma_{psf,2} = 0.025$ arcsec. The image noise is modelled as uncorrelated normally distributed pixel noise with vanishing mean and spatially constant standard deviation $\sigma_{n,pix} = 1$ (note that $\sigma_{n,pix}$ is used as surface brightness reference for the source and image surface brightness).

2.7 Radio images

...**t.b.d.**...

2.8 Data

Information on how to obtain the data can be found here: `sjhilbert.github.io/sllsc`. The optical images are provides as Flexible Image Transport System (FITS)[1] files. Additional information on known parameters and parameter priors are provided in an accompanying plain text file.

REFERENCES

Baltz E. A., Marshall P., Oguri M., 2009, J. Cosmology Astropart. Phys., 1, 015

Barkana R., 1998, ApJ, 502, 531

Bartelmann M., 1996, A&A, 313, 697

Bolton A. S., Burles S., Koopmans L. V. E., Treu T., Gavazzi R., Moustakas L. A., Wayth R., Schlegel D. J., 2008, ApJ, 682, 964

Despali G., Vegetti S., White S. D. M., Giocoli C., van den Bosch F. C., 2018, MNRAS, 475, 5424

Golse G., Kneib J.-P., 2002, A&A, 390, 821

Hellwing W. A., Frenk C. S., Cautun M., Bose S., Helly J., Jenkins A., Sawala T., Cytowski M., 2016, MNRAS, 457, 3492

Koopmans L. V. E., Treu T., Fassnacht C. D., Blandford R. D., Surpi G., 2003, ApJ, 599, 70

Navarro J. F., Frenk C. S., White S. D. M., 1996, ApJ, 462, 563

Navarro J. F., Frenk C. S., White S. D. M., 1997, ApJ, 490, 493

Neto A. F., et al., 2007, MNRAS, 381, 1450

Newton E. R., Marshall P. J., Treu T., Auger M. W., Gavazzi R., Bolton A. S., Koopmans L. V. E., Moustakas L. A., 2011, ApJ, 734, 104

Oldham L., et al., 2017, MNRAS, 465, 3185

Sawala T., Pihajoki P., Johansson P. H., Frenk C. S., Navarro J. F., Oman K. A., White S. D. M., 2017, MNRAS, 467, 4383

Sheth R. K., Tormen G., 1999, MNRAS, 308, 119

Wright C. O., Brainerd T. G., 2000, ApJ, 534, 34

[1] fits.gsfc.nasa.gov